Journal of South American Earth Sciences 87 (2018) 157–173

Contents lists available at ScienceDirect

Journal of South American Earth Sciences

journal homepage: www.elsevier.com/locate/jsames

Closure type effects on the structural pattern of an inverted extensional basin of variable width: Results from analogue models

Pamela Jara [a, *], Jeremías Likerman [b, c], Reynaldo Charrier [e], Sebastián Herrera [d], Luisa Pinto [d], Matías Villarroel [e], Diego Winocur [b, c]

[a] Departamento de Ingeniería en Minas, Facultad de Ingeniería, Universidad de Santiago, Chile
[b] Laboratorio de Modelado Geológico (LaMoGe), Instituto de Estudios Andinos Don Pablo Groeber, Universidad de Buenos Aires, Ciudad Universitaria, C1428EHA Buenos Aires, Argentina
[c] Laboratorio de Tectónica Andina, Instituto de Estudios Andinos Don Pablo Groeber, Universidad de Buenos Aires, Departamento de Ciencias Geológicas, Buenos Aires, Argentina
[d] Laboratorio de Modelación Analógica, Departamento de Geología, Facultad de Ciencias Físicas y Matemáticas, Universidad de Chile, Chile
[e] Escuela de Ciencias de la Tierra, Universidad Andrés Bello, Santiago, Chile

ARTICLE INFO

Article history:
Received 30 July 2017
Received in revised form
22 October 2017
Accepted 24 October 2017
Available online 28 October 2017

Keywords:
Analogue modeling
Tectonic inversion
Basin width
Closure style

ABSTRACT

In order to further understand the controls on the structural configuration of inverted basins, previous research has vastly explored the role of rift-stage stress field variations on the resulting structure produced by basin inversion. Analogue modeling has broadly enabled geoscientists to gain insight into the controls on the structural evolution during basin inversion, such as: the inherited structural array of the basin, sedimentary load or sedimentary thickness, plan-view shape of the basin (length and width), and variations on the governing stress field, among other factors. This work sheds light on the influence exerted by the closure style on inversion of an elongated model basin with a variable width, generated by differential extension. We subsequently induced inversion by modifying the orientation of the post-rift contractional stress field: (i) in a first model, contraction is homogeneous along-strike (parallel to the major axis of the basin); and (ii) in a second model, contraction is heterogeneous along-strike and exerted in the same orientation and amount in which extension was induced (about a pivot point). We focus on the three-dimensional geometry of the structures generated by inversion, their vergence and surficial trace, and where they are prone to concentrate within the basin, to finally analyze and compare our results with natural examples of inverted Andean basin systems. Our results indicate that most of the contractional deformation imposed in the analog models is absorbed in the interiors of the basin in its widest zones by means of inverted normal faults and backthrusts. However, when the amount of shortening is higher than extension, deformation is propagated outside the basin where shortcuts and new oblique reverse faults are dominant, which promote a major uplift.

1. Introduction

Along-strike variations in the structural pattern and evolution of the Southern Central Andes are ongoing subjects of debate (e.g., Charrier et al., 2007, 2015; Ramos, 2009). Our work is inspired by the abrupt changes in the structural trend and across-strike length of the Principal Cordillera and adjacent fold-and-thrust belt (FTB) systems (Fig. 1) (c. 32°–34° S), and attempts to contribute towards a better understanding of factors inherent to the uppermost-crustal structure of the overriding lithosphere that control such geometrical variations along the range.

In particular, between c. 32°-34°S, the Andean morphostructural segmentation (Fig. 1) is characterized by the development of the doubly-vergent Principal Cordillera, composed by Mesozoic and Cenozoic volcanic and sedimentary sequences (Charrier et al., 2002, 2007, 2015; Armijo et al., 2010; Farías et al., 2010; Jara and Charrier, 2014; Jara et al., 2015; Tapia, 2015), bounded towards the east by the thin- and thick-skinned, east-vergent, La Ramada, Aconcagua and Malargüe FTB's, which mainly involve Mesozoic rift sequences and generated Neogene syn-orogenic deposits (Kozlowski et al., 1993; Cristallini and Ramos, 2000; Giambiagi

* Corresponding author.
E-mail address: pamela.jara@usach.cl (P. Jara).

https://doi.org/10.1016/j.jsames.2017.10.018
0895-9811/

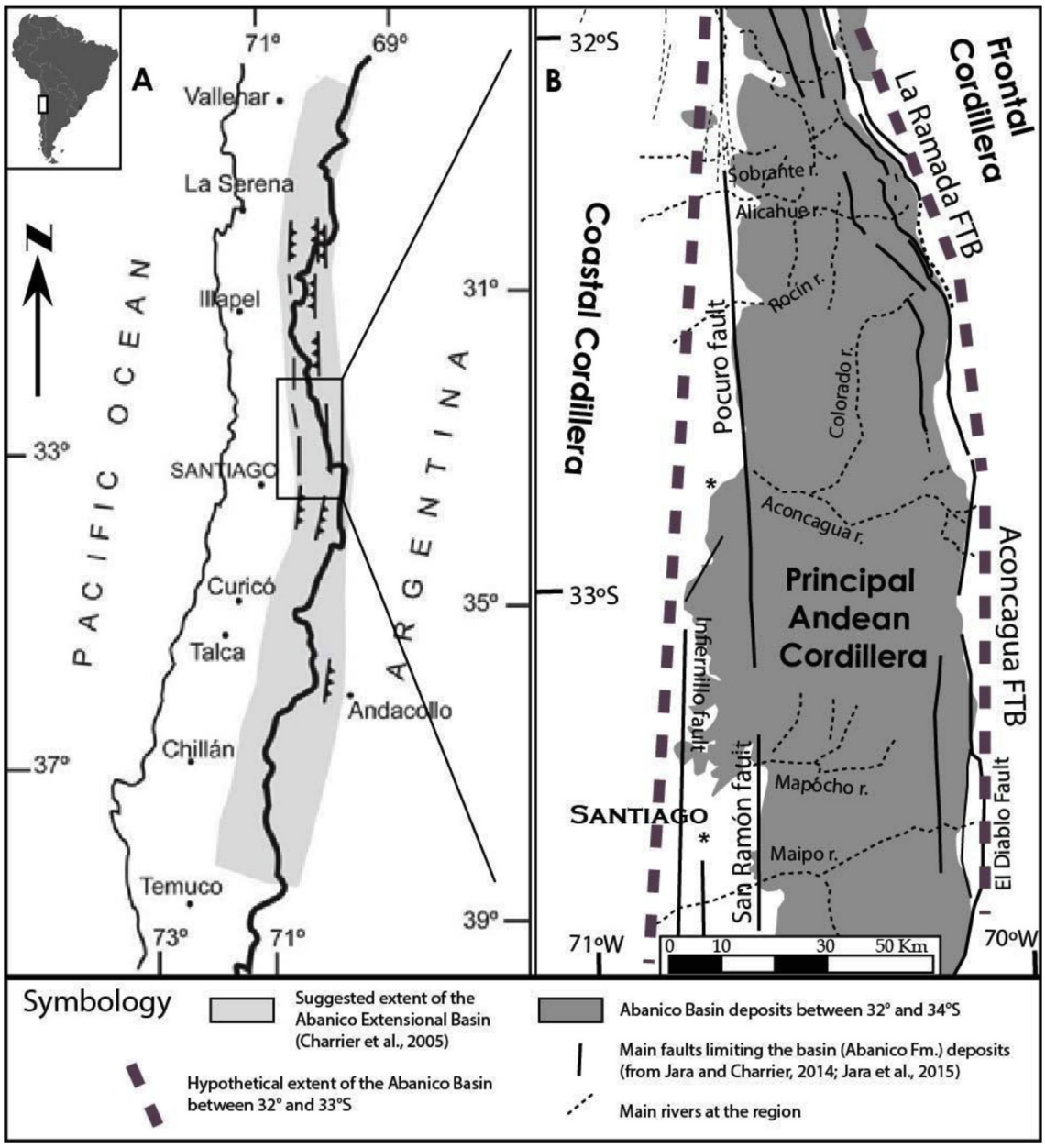

Fig. 1. Suggested extent of the Abanico Extensional Basin (A), and main trend of the structures that limits the basin deposits between 32° and 34°S (B). Note the NNW-SSE to N-S trend variation in the eastern border of the Principal Cordillera (B), the N-S to NNE-SSW change in the orientation of the Abanico basin at 33°S and the southward widening of the hypothetical extent of the Abanico basin (A) (Modified from Jara et al., 2015).

et al., 2003, 2012; Turienzo, 2010; Mescua et al., 2014, 2016). Limiting the FTB's at their eastern margin, the thick-skinned Frontal Cordillera (Ramos et al., 2002; Giambiagi et al., 2003; Mescua et al., 2016) exposes pre-Jurassic basement rocks and decreases its surficial expression towards the south, disappearing at c. 34°40′S, where the Malargüe fold-and-thrust belt progressively widens southwards (Kozlowski et al., 1993; Turienzo, 2010; Mescua et al., 2014), accompanied by an almost continuous decrease in horizontal shortening (Giambiagi et al., 2012) and by a linear decrease in orogenic volume (Pose et al., 2005). Moreover, at c. 34°S, strike of the Principal Cordillera main structures shifts from north to south, from ~N-S to ~ NNE-SSW, defining the Maipo Orocline (Farías et al., 2008; Arriagada et al., 2013).

Causes for the aforementioned variations in the upper-crustal Andean structure and its surficial expression have been attributed to both, plate interaction dynamics at the subduction zone, and the thermo-mechanical state of the South American lithosphere (Jordan et al., 1983; Isacks, 1988; Oncken et al., 2006). Influence of the latter on Andean mountain building has been related to rheological conditions of the overriding lithosphere, which are controlled by thermal flux, composition of the crust and its predeformed thickness (Tassara et al., 2006; Mescua et al., 2014). Furthermore, reactivation of preexisting weaknesses, such as suture zones or ancient structural systems is crucial in the resulting orogenic crustal structure and morphology (Ramos, 2009; Nemčok et al., 2013). Hereupon, the inherited structure generated by preorogenic extensional basins appears as a key control upon the development of orogens (Nemčok et al., 2013), and particularly, in the establishment of the different morphostructures that conform the Andean range (Dalziel, 1981). Just a few examples are: the

inversion of the Cretaceous Salta rift of northwestern Argentina (e.g., Carrapa et al., 2014); the inversion of Triassic and Late Jurassic-Early Cretaceous rifts in the Domeyko Cordillera of northern Chile (e.g., Amilibia et al., 2008); the inversion of the Cenozoic Abanico basin (Fig. 1) of central Chile (e.g., Charrier et al., 2002) among numerous others recorded along the range (e.g., Charrier et al., 2007; Martínez et al., 2012, 2015; Torres Carbonell et al., 2016).

Considering the relevance of inherited extensional rift basins upon orogenic systems development, it is necessary to define the three-dimensional geometry and kinematical aspects on the evolution of such basins, and to assess controls on their inversion mechanisms (closure style), given an inherited basin geometry. Basin evolution is generally characterized by along-strike segmentation into a series of isolated sub-basins (e.g., Corti, 2003; Bechis et al., 2009, 2014), defining heterogeneities regarding thickness of the basin infill and basin shape in plan-view. On the other hand, subsequent compressional phases may induce the reactivation of previous normal faults within the basin, contributing to a more complicated structural evolution due to inversion (e.g., Coward et al., 1991; Bonini et al., 2012; Jara et al., 2015). The complexity of positive tectonic inversion systems involves a number of controlling factors, such as, orientation of pre-existing structures (McClay and Buchanan, 1992; McClay, 1995; Yagupsky et al., 2008), the inherited geometry of the basin itself (e.g., Buchanan and McClay, 1991; Bonini et al., 2012; Martínez and Cristallini, 2017), dip angle of normal faults (e.g., Marques and Nogueira, 2008; Bonini et al., 2012; Sibson, 1985), the existence of lithospheric weaknesses and the older upper-crustal fabric (e.g., Bechis et al., 2014; Martínez and Cristallini, 2017), syntectonic sedimentation (Dubois et al., 2002; Pinto et al., 2010; Muñoz-Sáez et al., 2014), presence of fluids (Sibson, 1985), among other variables, discussed in detail by Bonini et al. (2012). Furthermore, previous observations on inverted basins (Jara et al., 2015) reveal a close relationship in between geometry of the basin and the concentration of deformation, quantity and style of the inversion-related structures.

Previous research identified marked along-strike differences in the structural pattern along the Abanico basin of central Chile (Fig. 1), and suggested that such changes were the result of the asymmetric closure of an extant extensional basin (Jara and Charrier, 2014). Based on this observation, a series of analogue models have been conducted in order to determine the differences in the structural patterns resulting from tectonic inversion in asymmetric basins under orthogonal and oblique compression leading to its closure. The results presented by Jara et al. (2015), led to suggest that basin width variations, significantly influenced the geometry of the structures developed during inversion. This work presents a second set of results that emerged from that previous study (using the same methodology) and with the objective of exploring the influence of the type of closure of a basin of variable width on the resulting structural pattern, during and after inversion. In order to assess the aforementioned, two main model setups were configured, carried out and compared.

It is worth mentioning that we do not particularly intend to compare our results in detail with natural examples world-wide, but to analyze them qualitatively considering several selected examples. We consider this contribution as a proxy for the study of natural inverted basins of different dimensions. As indicated by the conceptual model of Fig. 2, the general structural configuration within a basin system of a regional extent and variable width can correspond to a single basin or a set of major basins bounded by master normal faults, accompanied by second order (or minor) depocenters or sub-basins, distributed in a similar way regarding the major basins of the system (Fig. 2a). As observed in regional geological maps of South America, outcrop distribution of extensional basin deposits define asymmetric geometries in the plan-view (e.g. Ramos, 2009; Bechis et al., 2014), and likely, their hypothetical extent, prior to the latest Andean contractional phases, is also generally asymmetric. Therefore, asymmetry in the width of extensional Andean basins can be considered as an ubiquitous and common feature.

On the other hand, and due to the Andean regime, many of these basins have been tectonically inverted, resulting in altered structural patterns. We believe that, not only the inherited pattern of the basin (and other mentioned variables), but also the type of closure affecting the basin are first-order controls on the complex geometry in the structural pattern after inversion. Homogeneous compression (same amount of stress throughout the region) causes differences in the structural pattern generated by differential compression (Fig. 2b). Differential compression, without the influence of previous structures, usually generates a greater amount of shortening and uplift in the more compressed region, with a propagation of the deformation towards the foreland (Herrera et al., 2017). In this work, we show how the presence of the basin and basin closure kinematics play a fundamental role in the structural pattern generated by inversion.

We propose that by comparing the observed structural features resulting from basin closure style, the orientation of the stress field responsible for inversion of a natural prototype can be assessed. At the same time, based on the common characteristics observed in both types of experiments, and comparing this with natural examples, we would be able to: (i) infer the geometry of a natural prototype, and (ii) identify the areas that underwent a particular deformation in a naturally inverted basin (e.g., basin margins or interiors).

2. Methodology

2.1. Analogue models strategy

This work presents a second set of results obtained for inverted extensional basins models and evaluates the influence of the previous geometry of the basin and the orientation of the stress field controlling its inversion. The first set of results allowed to investigate the effects of width variations of an inherited extensional basin upon the structural features resulting from an overimposed contractional deformation stage. The analyzed features were the main structural trend, the number, geometry and vergence of generated structures, and the overall structural array during basin inversion (Jara et al., 2015). We used the same dimensions and scaling used in Jara et al. (2015), since it allowed us to make further comparison with prior results. In the present study, we aim to understand the influence of the type of closure of a basin whose opening was achieved by a differential (or inhomogeneous) extension (Fig. 2a). For the latter, we will close the basin (positive tectonic inversion) in such a way that the stress vector is applied in a direction perpendicular to the major central axis of the basin, thus generating homogeneous shortening in the region (Model A). Next, we shift the closure kinematics of the same basin generated in Model A, by imposing an equal magnitude of stress and direction, but in opposed sense regarding the aperture of the basin, thus inducing heterogeneous shortening along the major axis of the basin (Model B). After experiments are completed, we compare the experimental results of inversion of an extensional basin, where contraction was generated by: (i) homogeneous shortening (Model A), and (ii) heterogeneous shortening (Model B).

To generate a basin of variable width, and a non-homogeneous (heterogeneous) shortening, we have to apply the conceptual models of differential extension and compression (Fig. 2) of Jara et al. (2015). These conceptual models allow us to explain the

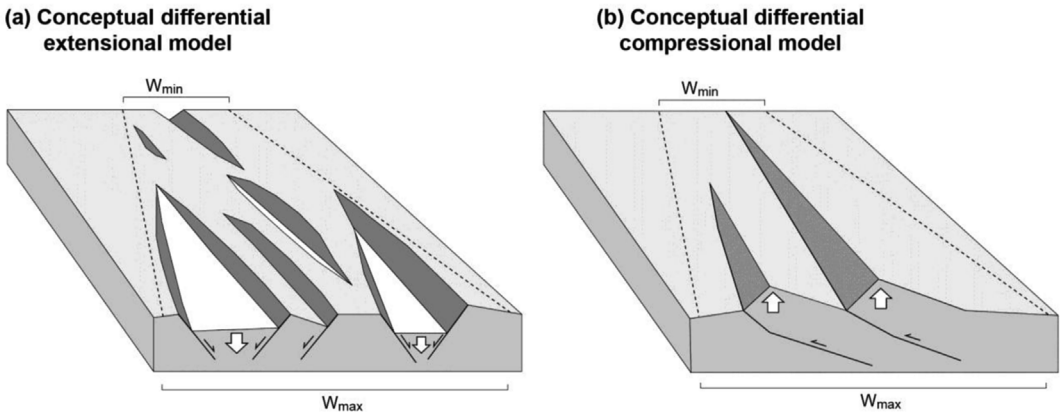

Fig. 2. Conceptual models of (a) differential extension and (b) differential compression. The vergence of structures is schematic and only referential. In both conceptual models there are no pre-deformational structures. The white arrows show the subsided (down) and uplifted (up) zones. The dotted lines correspond to the main deformation limits interpreted. W_{min} and W_{max} indicate the minimal and maximal width respectively (modified from Jara et al., 2015).

type of deformation that will affect our analogue models in the extensional stage of model A, and in the compressional stage of model B. Then, the starting point of both models (A and B) are a basin with variable width, similar to one of the model basins (Type I) of Jara et al. (2015). The difference in both models (A and B), in this contribution, is the type of closure of the basins, and how this affects the structural array after contraction. From these conceptuals models (Fig. 2) we consider that basins, in both A and B models, represent regions affected by differential extension, where main depocenters or sub-basins developed in the wider zone, whereas in areas that experimented less extension, isolated sub-basins were generated in a narrow zone (Fig. 2a). In a tectonic environment of differential compression (B Model closure style), the most shortened region will be the locus of greater uplift and the development of more compressional structures, compared to the area affected by minor shortening (Fig. 2b). Both conceptuals models correspond to a simplification, and hence did not considered pre-deformational structures or other factors. The models are explained in this section in order to show independently the type of opening and closing of the basins in our modeling.

Summarizing, the selected experiments are representative of two possible tectonic configurations. In model A, we investigate the influence of homogeneous shortening according to orthogonal convergence of a wedge-shaped rift basin, in presence of along-strike variations produced by differential extension (Fig. 2a) related to rotation about a pivot point. In model B, the same type of basin was inverted by progressively variating the convergence vector due to rotation about a vertical axis (same pivot used in the extensional phase).

To simplify results description and interpretation, we will refer to the widest part of the basin as its southern end (S), whilst the narrowest part of the basin would correspond to its northern end (N). Hence, extension increases progressively from N to S. In turn, in the case of inversion, model A considers closure by means of homogeneous contraction, perpendicular to the N-S direction; while a second experiment considers closure by means of heterogeneous contraction, applying compression in the exact magnitude, direction, but in opposite sense regarding the extensional stage. Thus, in the model B, compression increases progressively from N to S.

2.2. Scaling

In order to contrast analogue models with natural prototypes, experiments require proper scaling of the model parameters (Hubbert, 1937; Ramberg, 1981). The length ratio between model and nature will be $L = 10^{-5}$ (so 1 cm in the model will correspond to c. 1 km in nature). The gravity ratio between model and nature is $g^* = 1$, as both the prototype and the model are subject to the same gravitational acceleration. The corresponding stress ratio between model and nature is $\sigma^* = \rho^* g^* L^* \approx 6 \times 10^{-6}$. The scaling parameters used in the models for extension and compression are provided in Table 1. Although the experimental set-up lacked pre-rift brittle structures that may appear in nature, which can play an important role in the interaction and development of extensional structures (Sibson, 1985; Huyghe and Mugnier, 1992; Faccenna et al., 1995; Ranalli, 2000), emphasis was placed on the interaction between rift structures and those generated during subsequent shortening.

2.3. Set-up and materials

To induce differential extension and later heterogeneous or homogeneous contraction, the modeling apparatus of the experimental set-up (Fig. 3) included a fixed base, and a mobile basal plate fixed to a backstop (mobile wall) and connected to a step motor which displaced the mobile basal plate at a speed of 4 cm/h. In order to induce differential extension or contraction (Fig. 3), the mobile backstop was fixed to a pivot in its “northern” end. The angular velocity imposed on the backstop was 4°/h, and can be considered constant throughout the experiment (for more details see Soto et al., 2006). A maximum extension/shortening of 10 cm achieved in the area furthest from the pivot point for all the models.

Above the basal plates of the apparatus, a stratified 3 cm-thick sand pack was manually deposited, in an extent greater than the plate dimensions, to hinder “edge effects”. We used rounded, low-cohesive (100 Pa) quartz sand with an internal frictional angle close to 32.7° to model the brittle behavior of upper-crustal rocks (Hubbert, 1951). A thin layer of silicone (SGM36) was used to cover the velocity discontinuity zone (VD in Fig. 3), in order to distribute strain in a wider space and allowing the generation of multiple structures instead of a single pair from the velocity discontinuity. SGM 36 is a Newtonian viscous silicone manufactured by Dow Corning, which has a density of 965 kg m^{-3}, and an effective viscosity of 5×10^4 Pa s at room temperature (20 °C). In these experiments, the silicone does not simulate any element of the crust and has been used with the purpose of generating space for extension resulting from deformation (as in Brun and Nalpas, 1996; Pinto et al., 2010; Muñoz-Sáez et al., 2014), allowing strain to be distributed and thus creating a wider deformation zone. This layer had a wedge shape, similar to that generated by the movement of the mobile

Table 1
Scaling parameters for models A and B, in both extensional and compressional phases.

	l (m)	g (m/s^2)	ρ (kg/m^3)	μ (Pa s)	V (m/s)	σ (Pa)	ε (s^{-1})
Nature	1000	9.81	2300	1.8×10^{21}	5×10^{-13}	2.2×10^{7}	10^{-14}
Model	0.01	9.81	1400	5×10^{4}	1.1×10^{-5}	1.4×10^{2}	2.2×10^{-3}
Model/nature(*)	10^{-5}	1	0.6	2.7×10^{-17}	$2{,}2 \times 10^{7}$	6×10^{-6}	2.2×10^{11}

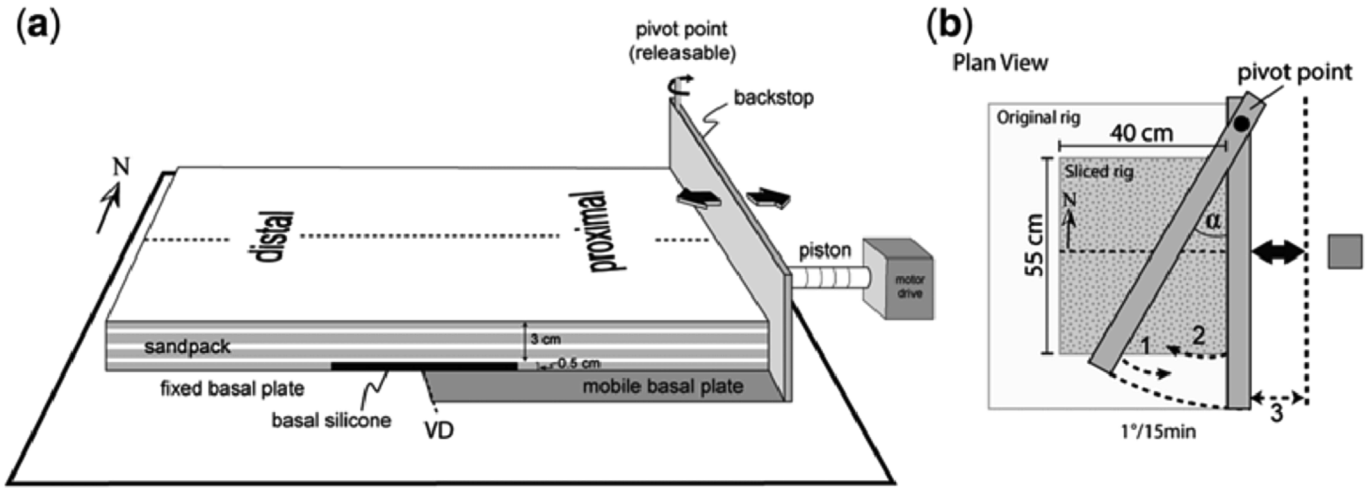

Fig. 3. (a) Model set-up. The proximal and distal zones are defined by the relative distance regarding the backstop, and used in the models description (b) Plan view and backstop kinematics: α, angle of backstop rotation; 1, differential extensional movement by applying backstop rotation; 2, differential compressional movement by applying backstop rotation; 3, homogeneous (orthogonal) movement of the backstop by releasing the pivot. Movements 1 and 3 are applied in inversion of Model A. Movements 1 and 2 are applied in inversion of Model B (Modified from Jara et al., 2015).

basal plate, but extending beyond the limits of the VD. This geometry was tested previously (Jara et al., 2015), and selected after comparison with a silicone layer of larger size and rectangular shape, for which more material was used, but the effect on the geometry of the structures of the extensional system resulted the same. Benchmarks for the use of SGM 36 in analogue modeling has been established by several authors (e.g., Weijermars, 1986; Davy and Cobbold, 1991; Schellart and Strak, 2016); it represents an analogue for materials with viscosities between 10^{18} and 10^{21} Pa s, which is sufficiently similar to those commonly used for high detachment viscosities (Van Keken et al., 1993; Weijermars et al., 1993).

2.4. Experimental procedure

Each experimental run consisted of two stages, an initial extensional stage (1 in Fig. 3b), and a subsequent contractional stage. Heterogeneous contraction (contractional stage in Model B) was generated by means of a pivotal movement (2 in Fig. 3b), whilst homogeneous contraction (contractional stage in Model A) was applied by releasing the mobile wall from the pivot point (3 in Fig. 3b).

Opening of the basin during the extensional stage was recorded by high-resolution photographs taken in regular time intervals to analyze the surficial structural development of the model. Likely, the model surface topography was recorded by a c. 0.135 mm vertical accuracy laser scan in regular time intervals. The obtained data was processed to remove spurious values. Subsidence was calculated from the incremental difference between successive gridded data. Once extension was completed, the step motor was paused, and accommodation space generated by extension was filled up with brown colored sand replicating synrift sedimentation. At the end of all the experiments, dry sand was sieved onto the model's surface to preserve the final topography. To register the resulting three-dimensional geometry of the extensional stage, some models were cut to observe the internal structural array previous to inversion. Cut models cannot be used again, so 4 extensional models were made. Two of them were cut and studied in their evolution, and allowed us to verify that the resulting geometry of the basin is not an effect of the limits of the basal silicone (we use wedge-shaped and rectangular geometry to compare). The other two corresponded to the initial (extensional) stage of the compressed models.

Closure of the basin by homogeneous contraction was accomplished by releasing the mobile basal plate and the backstop from the pivot, and subsequently inverting the basin (Fig. 4a). In the case of heterogeneous contraction, inversion was achieved by inverting the direction of motion of the stepmotor (Fig. 4b). As for the extensional stage, the superficial structural evolution and topography variations during inversion were carefully registered. In order to obtain cross-section views of the final models, and a three-dimensional view, the models were cutted after the extensional and compressional phases were completed. Cutting the deformed sand packs was carried out by coating the models in a hot gelatin solution and, once cooled and slightly hardened, sliced in c. 5 mm sheets, orthogonal to the main structural trend. The sand that filled the grabens prior to inversion acted as marker of deformation, and could be identified because it was not stratified. Moreover, synrift sand deposits on the hanging wall of normal faults are thicker than on the equivalent footwall, so inversion will show thicker packages of synrift material lifted upon the hanging wall of positively inverted faults.

3. Results

3.1. Extensional stage: basin with variable width by means of differential extension

During the extensional stage in both models (Fig. 5a), we

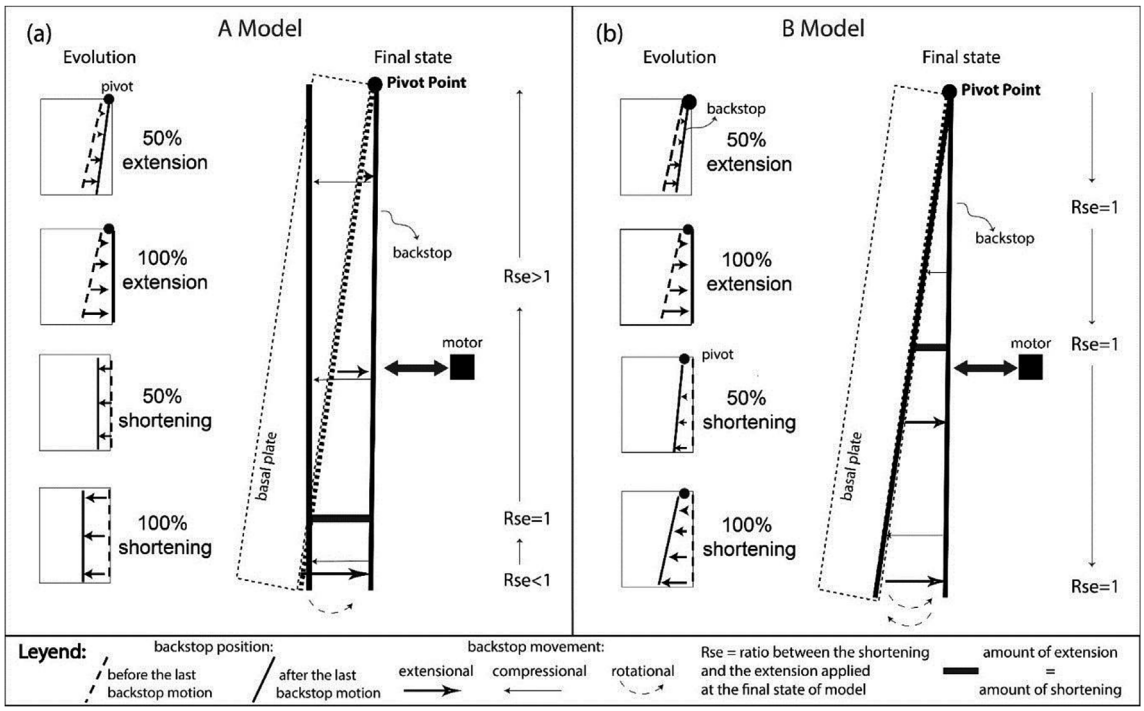

Fig. 4. Scheme of the model kinematics. (a) Orthogonal inversion relative to the longitudinal (N-S) axis of the basin ("Model A"), and (b) differential inversion generated by inducing closure of the basin in the same magnitude and sense, but in the opposite direction in which extension was induced ("Model B"). (Modified from Jara et al., 2015).

observe that the basin initiated its opening in its northern end, close to the pivot point, marked by the generation of a narrow graben bounded by a pair of ~N-S trending normal faults, with opposite dips (at 25% of extension). Despite the fact that the basin aperture begins in this area, we note that the final amount of extension in the northern end of the model was the minimum. During subsequent stages (at 50–75% of extension), new normal faults were generated, concentrated in the internal area of the basin (along the basin axis), and progressively towards the proximal zone (close to the backstop). These normal structures presented a main N-S trend, with the exception of the bordering structures of the basin, which developed with slightly oblique trends, ~NNW-SSE and ~NNE-SSW, along the proximal and distal zones, respectively. These bordering structures, however, only controlled space generation in areas where the basin was narrower (towards the northern end of the basin), in the central and southern zones of the basin there is not a great development (activity) of these faults in the first stages of extension (Fig. 5a). Major space generation developed in the inner areas of the basin, clearly represented in the model cross-sections (Fig. 5b), where deeper and wider grabens were formed. Grabens in the model were distributed along the innermost zone of the basin, concentrated along the basin axis and controlled by normal faults with restricted along-strike continuity, allowing the creation of isolated depocenters, which, in some cases, are connected by relay ramps (Fig. 5a and b). In the widest area of the basin (towards the southern end), bordering structures of the distal zone did not exert a prime role in space generation, as they experience minor (if not null) displacement. However, along the proximal zone, the bordering normal structure experienced important displacement, thus accommodating extension and related subsidence (Fig. 5a and b). Both bordering structural systems allowed the recognition of the zone of distribution of extensional deformation.

3.2. Contractional stage

3.2.1. Model A: inversion by means of homogeneous compression

The contractional stage of Model A resulted in homogeneous shortening of the extensional basin. Inversion was accomplished by applying contraction in a direction orthogonal to the N-S axis of the model (Figs. 4a and 6), and in an amount equal to the amount of extension in the southernmost (widest) part of the basin. Thus, the inversion ratio (Rse = ratio between the shortening and the extension applied at the final state of model; see Fig. 4) will be progressively greater than 1 from the southern end towards the north (Figs. 4a and 6).

Most relevant features of this model are described in the following. We emphasize the characteristics that allows us to contrast the results of this model with the ones obtained in Model B. One of the most prominent features resulting from Model A was an uplifted zone, which experienced topography increments during the whole contractional stage, controlled by oblique (in map-view) reverse faults generated beyond the basin borders, therefore not being directly related to previous normal faults, but closely related to the presence of the basin. Final state cross-sections of this experimental run (Fig. 6), show that the new reverse faults have greater vertical throw towards the narrow zone of the basin. In contrast, towards the widest zone, vertical throw within new reverse faults diminished progressively southwards until they become absent. The latter suggests that zones of concentrated contractional deformation are intimately related to the inherited geometry of the basin. Several normal faults generated during the extensional stage were preserved and some only partially reactivated. Thrusting inside the narrowest (northern) segment of the model, was totally concentrated inside the basin domain, and in the external proximal zone (Fig. 6a). In both mentioned areas, deformation is absorbed by N-S to slightly oblique trending structures.

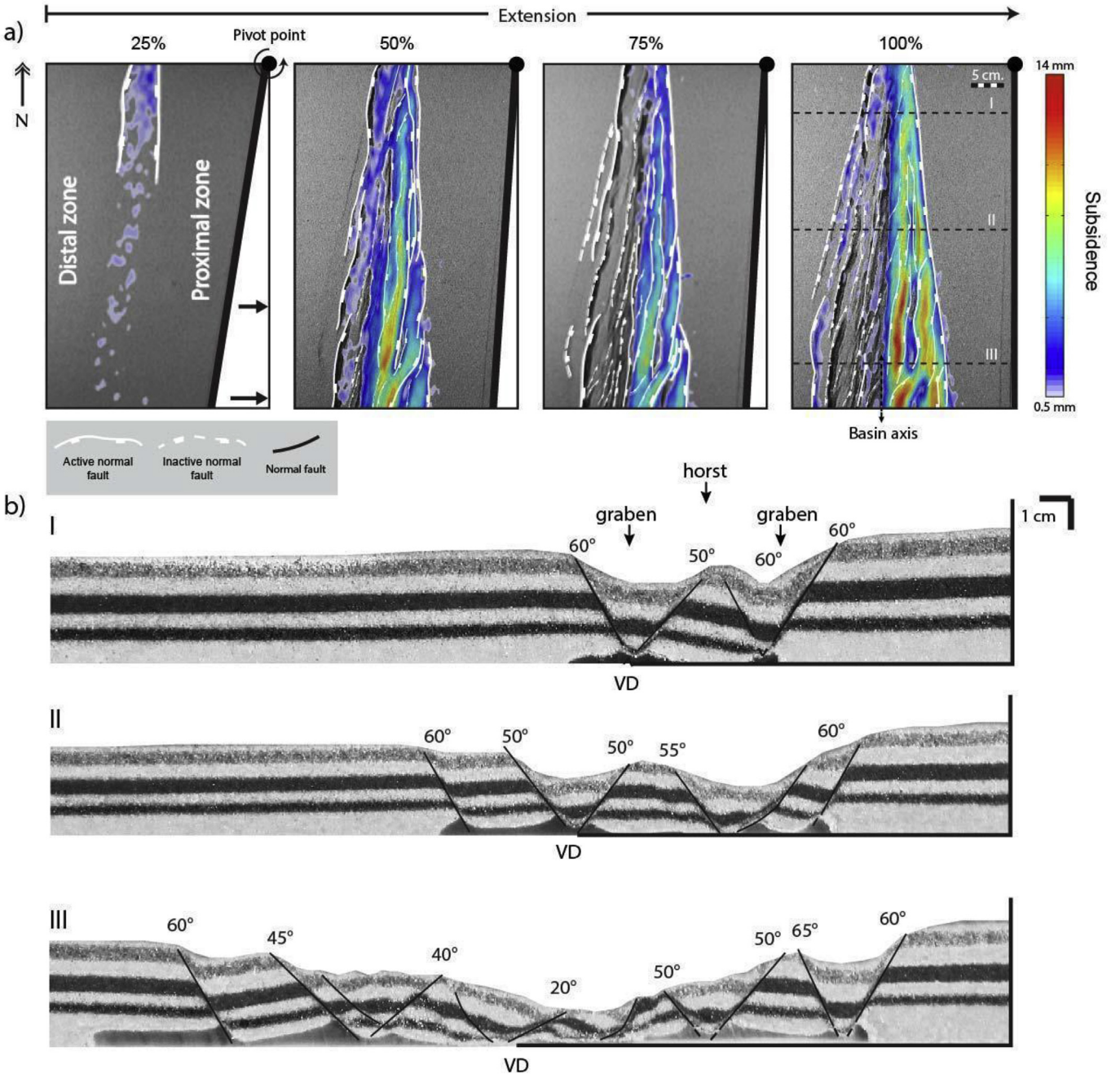

Fig. 5. a) Plan-view of the extensional stage in both models (A and B), showing structural development and relief evolution b) Cross-sections at three latitudes (N, center and S) after the extensional stage. Resulting structures are outlined and fault dips are specified. VD: velocity discontinuity. (Modified from Jara et al., 2015).

On the other hand, different areas of the basin were inverted by means of displacements along essentially N-S trending reverse faults, which generated a maximum amount of uplift in the vicinity of the basin axis. Furthermore, cross-sections (Fig. 6b) showed that the basin borders are only crucial in the narrow area of the basin (northern zone), thus allowing extrusion of the basin infill by means of border-fault inversion. This reverse reactivation of normal faults generated a pop-up structural array, characterized by short-cut thrusts nucleated in the reactivated structures (Fig. 6b). In the southern zone, were the inverted basin was originally wide, inversion is mainly controlled by opposite verging thrusts, generating a triangular zone in which former normal structures of the extensional stage are transported towards the interior of the basin, and preserved within thrust fault-propagation folds (Fig. 6b).

3.2.2. Model B: inversion by means of differential compression

The contractional stage of Model B generates inversion of the basin by means of a pivotal closure mechanism that mimics the kinematics of the extensional stage, but shifting the direction of movement of the backstop to the opposite sense. Thus, the exact amount of shortening compared to extension is imposed ("scissor style" closure; Fig. 4b), resulting in a generalized Rse = 1 for the whole basin.

The main observation in the plan-view evolution of Model B, is that contractional deformation is concentrated within the limits of the extant basin, and that shortening is mainly absorbed along the

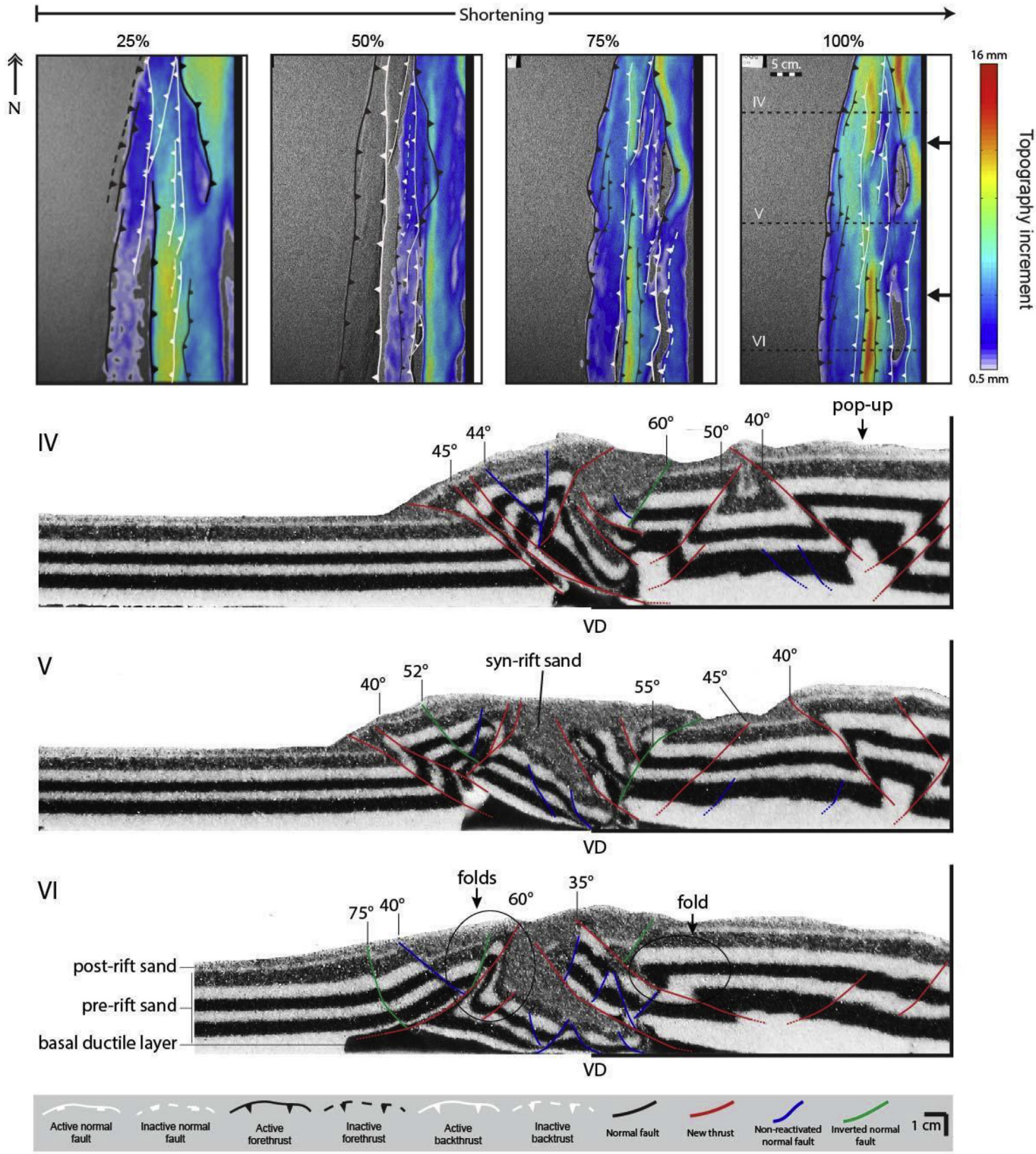

Fig. 6. a) Plan-view of the contractional stage in Model A, showing structural development and relief evolution. b) Cross-sections of Model A after the contractional stage (IV, V and VI). Resulting structures are depicted and fault dips noted. Location of the transects are outlined in 6a. (Modified from Jara et al., 2015).

basin axis, forming N-S trending faults (Fig. 7). Where uplift reached a maximum, shortening was also the greatest, coinciding with the originally widest zone of the basin (Fig. 7).

Not all extensional structures were inverted, and new reverse faults and associated folds were generated (Fig. 7). The newly formed reverse faults affecting areas outside the original basin were only formed were shortening reached high values. In the northern end of the inverted basin, a pop-up structure bounded by inverted previous normal faults absorbed contraction and allowed "extrusion" of the basin infill. Inside the pop-up, new reverse faults occurred and non-reactivated normal faults were preserved along the axial zone of the inverted half-graben. In the southern domain

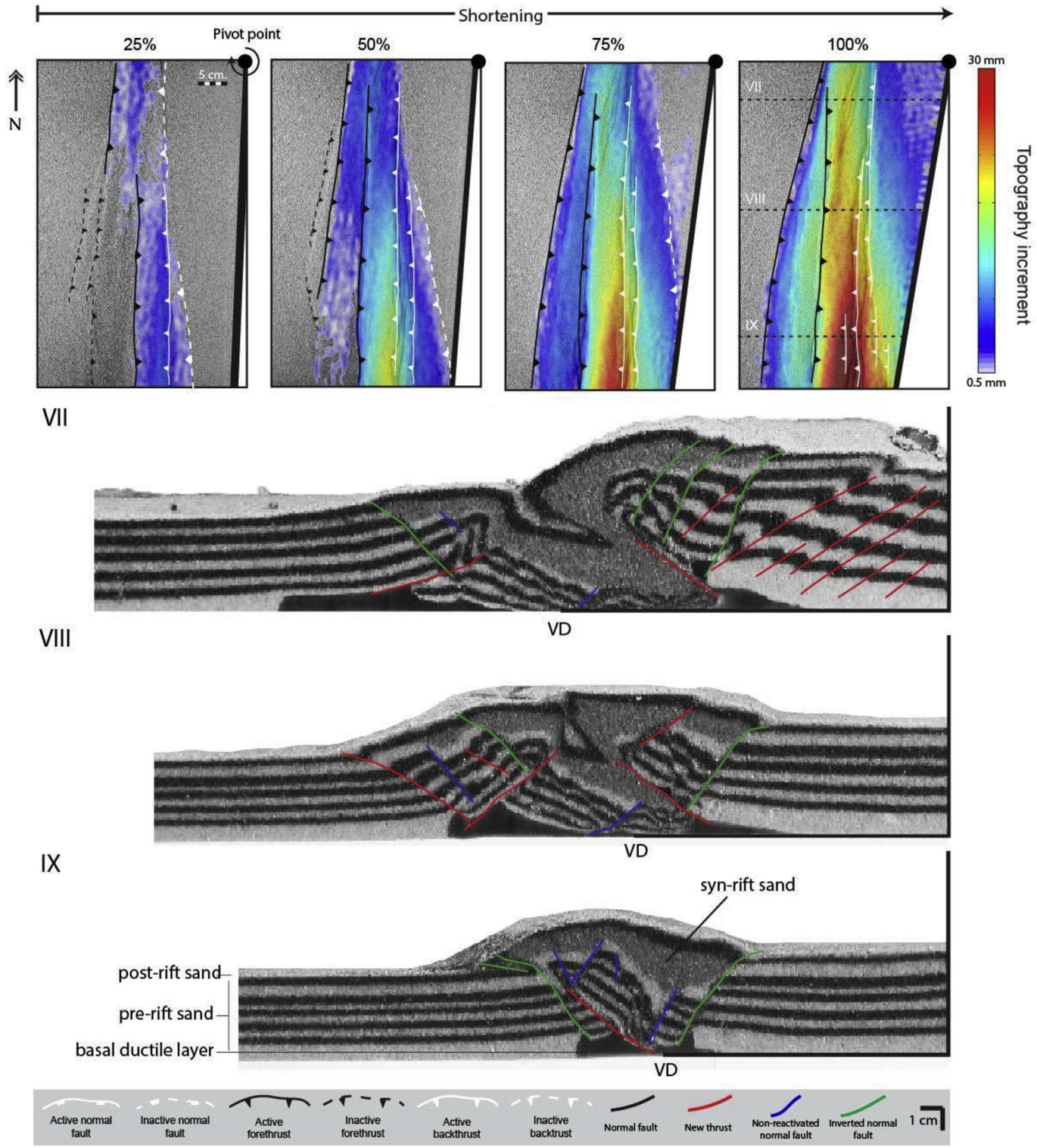

Fig. 7. a) Plan-view of the contractional stage in Model B, showing structural development and relief evolution. b) Cross-sections of Model A after the contractional stage (VII, VIII and IX). Resulting structures are depicted and fault dips noted. Location of the transects are outlined in 7a.

of the basin, normal faults were preserved, and surface uplift during inversion was controlled by newly formed reverse faults. These new reverse faults showed opposite dips, taking advantage of the bordering normal structures formed during extension. The reverse faults transported the external areas of the basin towards its interiors, constituting a pop-down within a triangular zone. Furthermore, backthrusts are present in the proximal area (towards the backstop).

3.3. Comparative analysis: homogeneous vs. differential compression

In both models, compression was superimposed to a basin of variable width with a similar overall geometry and structural

features. As the extensional phase for both models was equal, and contraction was exerted differentially, the differences caused by the type of closure during inversion were assessed.

The main differences between the results reside in the distribution and style of newly formed reverse faults during inversion, and the reactivation or preservation of normal faults. In Model A, non-rotational oblique reverse faults were generated where Rse>1 (narrow zone of the basin), beyond the limits of the original basin. These structures were active throughout the entire stage of contraction (Fig. 6). In Model B, such structures are not observed, and inversion is mostly concentrated within the limits of the original basin, except for the wide zone, were reverse faults are generated in the proximal area of the model. In the latter area, block rotation (about a vertical axis) occurred along the newly formed reverse faults (Fig. 7). In the northern zone of Model B, normal bordering structures were inverted, generating a pop-up containing non-reactivated secondary normal faults (Fig. 7).

In both models, N-S trending newly formed reverse structures were observed in the interior of the basins, and were more active in the depocenters generated during the extensional stage, where the basin attained a larger width. New reverse structures not related to former normal faults, as well as partially-inverted or non-reactivated normal faults occurred in both models. Moreover, in models A and B, uplift of the basin infill was controlled by a doubly-vergent structural system. Normal faults in the center of the basin facilitated propagation of deformation towards the surface by means of their reactivation during inversion.

Propagation of deformation in both models is somewhat difficult to observe, since a “normal” in-sequence migration towards the distal zone did not occur, as expected. Instead, deformation during inversion was concentrated within the basin limits and then, transferred towards the proximal zone. Contraction in the proximal zone was evidenced by topography increments (Figs. 6 and 7), and was generated by the growth of pop-up structures, as observed in the cross-sections of Figs. 6 and 7. However, only in the case when the amount of shortening surpassed the amount of extension, contractional deformation was observed beyond the basin limits, always restricted to its vicinity.

Preserved normal faults generally have dips of 60°; while those that have been reactivated, show dips ranging 55°–50° in depth. However, in surface, fault dips diminish to 30° or 25°. The reverse faults (new thrust faults) have dip angles of 30°–45°, several of which increase or decrease towards the surface, and, in some cases decrease notoriously in depth until becoming subhorizontal at the detachment level. Note that new thrusts dips in model A are greater than in model B (Figs. 6b and 7b), which might be due to the fact that the structures of model A have almost N-S strikes resulting from the orthogonal compressive stress.

In general, we observe that shortcut faults are mainly responsible of the absorbed shortening in Model A, while backthrusts become important in Model B. Along the narrow (northern) zone of both models, the bordering normal structures exert a fundamental role during inversion, uplifting the basin infill by reactivation as inverse faults, and hampering the generation of new reverse faults.

The schemes shown in Fig. 8 outline and summarize the main features that allows us to compare the final results of both models. In Model A (Fig. 8a), major uplift is concentrated in the northern proximal zone, and uplift in the southern sector is smaller, where compressive deformation is distributed by more reverse faults in the region where the previous basin was wider. On the other hand, in Model B (Fig. 8b), major uplift is concentrated in the southern proximal zone, and uplift in the northern sector is smaller, which is expected since the amount of shortening was higher in the southern sector. Even so, note the vergence and how deformation is distributed (Fig. 8b), which differs from the conceptual differential compressional model (Fig. 2b), expected in the case where there is no previous basin.

4. Discussion

4.1. Results summary

In general, the structural array resulting from the experiments is comparable to structural features observed in natural prototypes of inverted basins. These comparisons should allow to: (1) determine the style of closure of a natural prototype (homogeneous or heterogeneous closure); and, for each case, (2) to identify areas where a natural prototype had an important extensional development in a broad or wide zone, composed by isolated depocenters controlled by normal faults, or, conversely, if the natural prototype had a less important extensional development in a narrower zone.

During the development of both models, we observed that the presence of the basin plays a fundamental role during compression, when inversion occurs, since most of the deformation is concentrated within the margins of the pre-existing basin. Minimum propagation of deformation towards the distal zone is registered (Fig. 9). This is observed in model B, where shortening towards the south is greater than in the northern region, where migration of deformation towards the distal zone could be expected (Fig. 2b).

From the results of our models, it can be inferred that once the basin is completely inverted and the basin infill was uplifted, tectonic transport beyond the margins of the original basin (especially towards the distal zone) is greatly hampered. At this moment, the inverted basin infill begins to behave as a very rigid block that resists further contractional deformation. In the proximal zone, pop-up structures accommodate contraction beyond the uplifted block, which was observed as the progressive development of a bulge in the proximal zone during contraction.

The normal faults in both extensional models have a dip close to 60° in the basin borders areas (Figs. 6 and 7), dip that decrease towards the interior of the depocenter. We note that de dip angle wasn't a fundamental factor in the selective of faults to be reactivated during the inversion process, since faults in a similar position into the basin (and similar dip angle), were reactivated in one model and no reactivated in the other. Moreover, faults with similar dips angle at the same basin, were or not reactivated in relation to their position into the basin. Therefore, we can infer that in our model de dip angle of the faults don't play a fundamental role in the selective inversion of faults, but the basin width and the type of closure of the basin.

The comparative chart on Fig. 9 allows to visualize some of the main differences that we observe in the final results of both models. The figure highlights some of the main features (detailed in the following paragraphs) that allow us to compare our models to some natural prototypes given as examples in the 4.2 section.

4.2. Main characteristics of the models and comparison with natural cases

4.2.1. Preserved, reactivated or news structures

One of the aforementioned features recognized in both types of models, is the generation of new sets of reverse faults, and the preservation of partially- and/or non-reactivated normal faults throughout the inverted basin. The preserved, reactivated and new reverse faults are shown regarding their relative importance during inversion (Fig. 9), according to their generation during contraction (Figs. 6 and 7). To interpret the location of the previous basin, we need to complement this information with other data such as the location of the border faults of this inherited basin, in relation to the zone affected by compressive deformation, which is different in

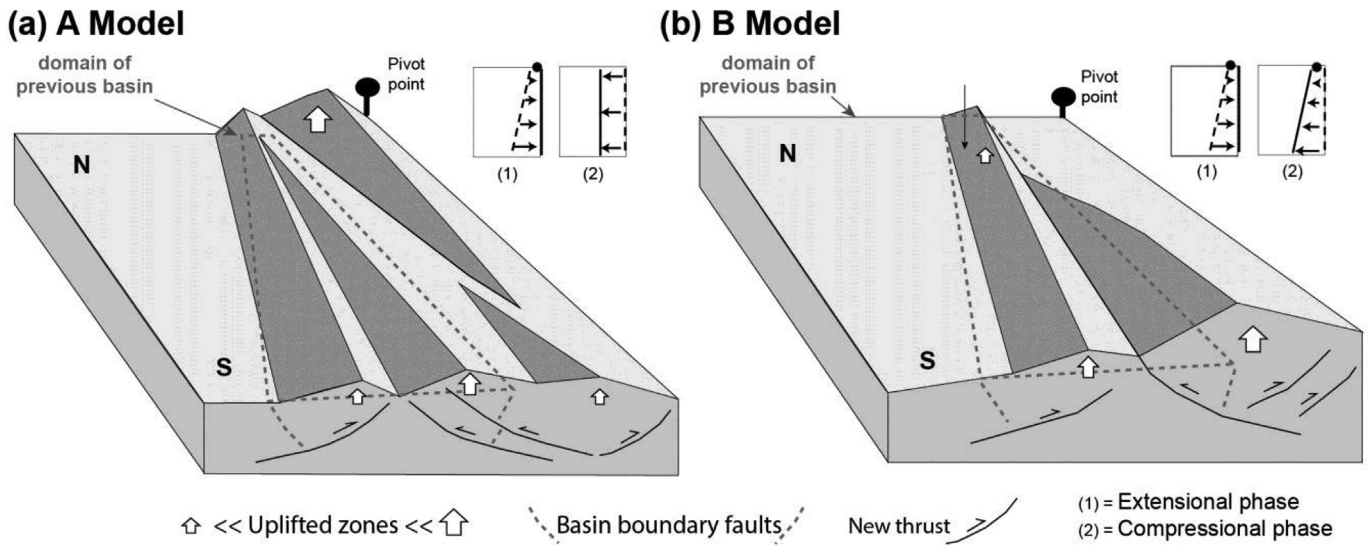

Fig. 8. Conceptual models based on the results of inversion of a basin with variable width, by means of (a) homogeneous compression and (b) differential compression.

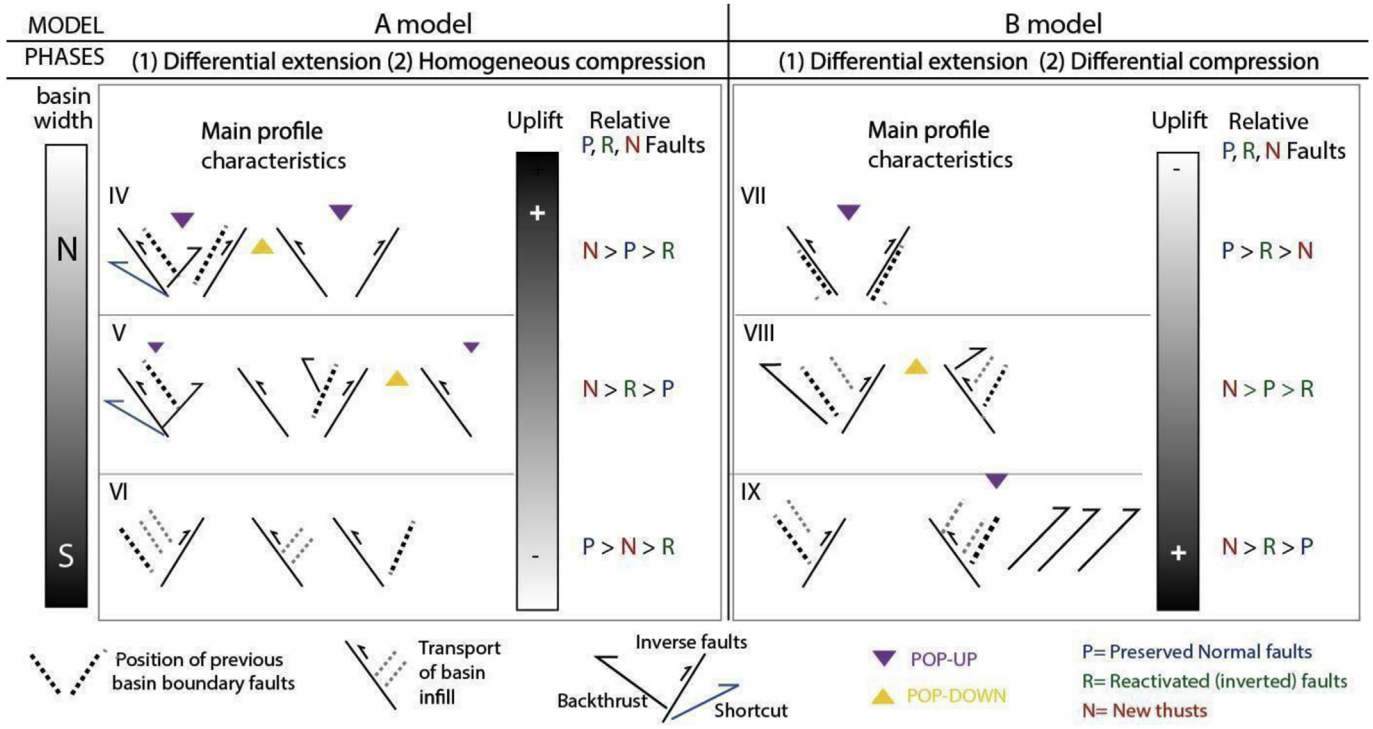

Fig. 9. Comparative chart of the main characteristics in the profiles of both models at similar latitudes (N, center and S relative to previous basin). For details see Figs. 6 and 7 (IV, V, VI of A model and VII, VIII and IX of B model).

both models (Fig. 9).

Preserved, reactivated and new reverse faults have been observed in natural prototypes of positively inverted basins, along several Andean provinces and other orogens. Such structures were registered by Eubank and Makki (1981) in the Moroccan "Sunda folds", where in a set of faults of similar orientation, some structures suffer reactivation and others do not (Fig. 10). Brun and Nalpas (1996) and Yagupsky et al. (2008) explained this occurrence as a consequence of the orientation of the inversion stress field regarding the extant normal structures of the basin; this is, reactivation is hampered when previous faults are orthogonal to the main stress direction, and facilitated when the orientation of these faults is slightly oblique to the main stress direction (~15°). Similar observations were pointed out by Yagupsky et al. (2008). However, partial and null reactivation of former normal structures, regardless of their orientation, is considered as a common phenomenon during positive basin inversion (Lowell, 1995). In this study, normal faults without positive reactivation are present in both models, and occur in the wide and narrow zones of the basins. Nevertheless, they are always concentrated in the interiors of the basin, close to the center (Figs. 9 and 10). Furthermore, in both types of models, the bordering structures are partially inverted, suggesting that

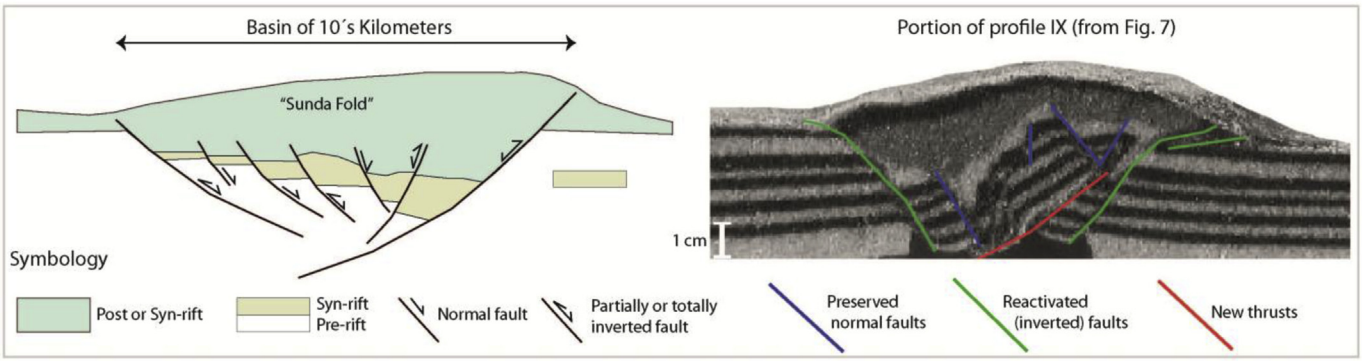

Fig. 10. Schematic diagram showing similarities in preserved, reactivated and new faults developed in a natural example ("Sunda folds", modified from Eubank and Makki, 1981) and in the narrowest zone of model B.

partially inverted normal faults within a natural prototype could correspond to basin margin structures, or likely related to the borders of the basin. Moreover, if these faults correspond to bordering structures, responsible in great part for inversion of the basin (uplift and exhumation of the infill), they could have developed in the narrow zone of an asymmetrical basin (profiles IV and VII in Fig. 9, and Fig. 10).

4.2.2. Pop-up and pop-down structural array

From the results of our models, it can be inferred that once the basin is completely inverted and an uplifted core is generated, tectonic transport beyond the margins of the original basin (especially towards the external or distal zone) is greatly hampered. At this moment, the inverted basin starts to behave as a very rigid block that resists further contractional deformation. In the zone comprised by the uplifted block, together with the mobile wall (proximal zone), pop-up structures absorb the shortening that was not accommodated within the uplifted block.

The pop-up and pop-down arrays are simply the result of an encounter of two inverse faults of opposite vergence, defining a triangular zone. Pop-ups are common in both models (Fig. 9), and specifically, where the inherited basin was narrow (and thus Rse > or equal to 1). In model B, the pop-ups are distributed in several regions (Rse = 1). This allows us to interpret that the presence of triangular zones in natural basins could indicate regions where the basin was narrow, or where the amount of shortening exceeded that of previous extension after positive inversion.

The pop-up style in positive basin inversion is generally present in natural prototypes, such as in the Cuyo depocenter of western Argentina (Uliana et al., 1995), in complex structural arrays registered in the French Western Alps (Coward et al., 1991), in the Domeyko Cordillera of northern Chile, and the Valle del Cura Basin at the Frontal Cordillera in central Argentina, where inverted grabens have been registered in detail (Amilibia et al., 2008; Winocur et al., 2015). Natural basin prototypes that appear to have experienced minor extensional development, and a lesser amount of shortening related to inversion regarding adjacent areas (e.g., La Pilona cross-section of Giambiagi et al., 2015), could be specifically related to narrow basin zones (Fig. 11). The major importance of the "pop up arrangements" reside in that they can raise the basin infill together with associated inherited structures (preserved normal faults), as observed in profiles IV and VII (Fig. 9) and in several natural prototypes besides the aforementioned (e.g., Bonini et al., 2012).

Moreover, the pop-down geometry observed in our models is comparable with reverse faults and associated folds of opposite vergence towards the interior of the Salta Rift Basin, inverted during the development of the Eastern Cordillera in northwestern Argentina (e.g., Filo Paranilla and Las Minas anticlines in Carrera et al., 2006). These natural fault arrays exhibit remarkable similarities with the wide zones of models A and B.

4.2.3. Transport of the basin infill

Reverse faults that tectonically transport the basin infill, together with preserved normal structures (not- or partially-reactivated), occur in the wide zone of both models. Tectonic transport, in both cases, is towards the interior of the basin, and by means of newly generated reverse faults, dipping in opposite direction regarding the normal structures that controlled basin development. Tectonic transport, as aforementioned, has been observed in the Cacheuta basin of western Argentina (Cacheuta cross-section of Giambiagi et al., 2015, Fig. 12), in which several normal structures are preserved within an anticline, in a zone that experienced major shortening compared to an adjacent area. The preservation of normal structures within inverse fault-related folds is comparable to what is observed in the wide zone of Model B (Fig. 9), suggesting that the Cacheuta basin (Giambiagi et al., 2015) might correspond to a basin of variable width that was subjected to inversion by means of heterogeneous contraction, similar to the closure mechanism of Model B. Other comparable features can be observed in the Salta Rift of northwestern Argentina, specifically in the "Quebrada La Yesera" cross-section of Carrera et al. (2006). In this inverted rift system, normal faults (e.g., La Yesera extensional fault) are preserved and juxtaposed to inversely reactivated normal faults (e.g., El Zorrito-Las Chacras thrust).

4.2.4. Basin boundary faults

In the wide zones of our model basins, the bordering structures generated during extension do not chiefly absorb contractional deformation during inversion (profiles VI and IX in Fig. 9). This appears to be in contradiction regarding classic models of basin inversion, in which inversion within a hemi-graben is accomplished by contraction of the hanging wall (McClay and Buchanan, 1992), accompanied by the generation of an harpoon-style anticline defined by the deformed sedimentary infill of the basin margin (McClay, 1995; Bonini et al., 2012). This main difference can be caused by the pre-imposed nature of the basin margins in the classic models mentioned above; in which the orientation and location of bordering structures is pre-defined by means of rigid blocks of a determined geometry (Fig. 12a) to simulate the pre-extensional failure of basement rocks. Therefore, the models presented in this study are more comparable to natural examples that occur in regions where normal faults controlling basin

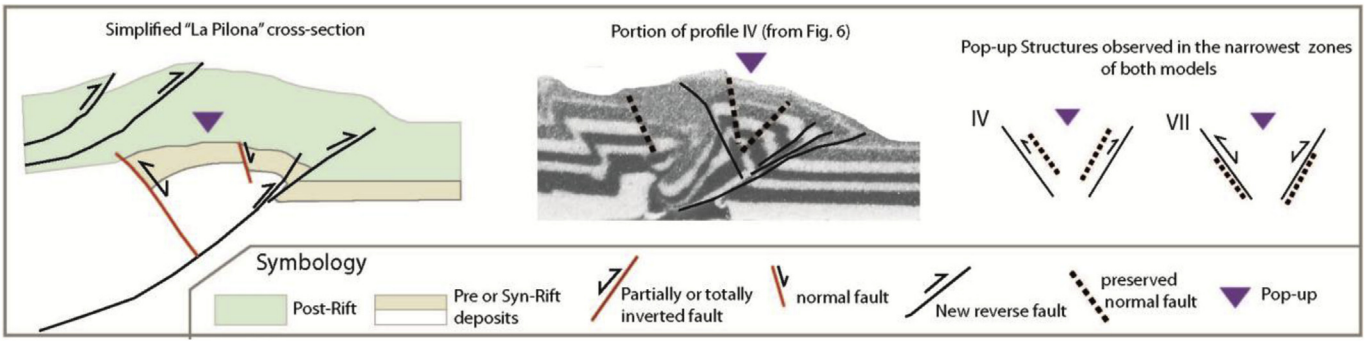

Fig. 11. Schematic diagram of pop-up structures observed in a natural case (La Pilona cross-section modified from Giambiagi et al., 2015) and in model A (profile IV) and B (profile VII) from Fig. 9.

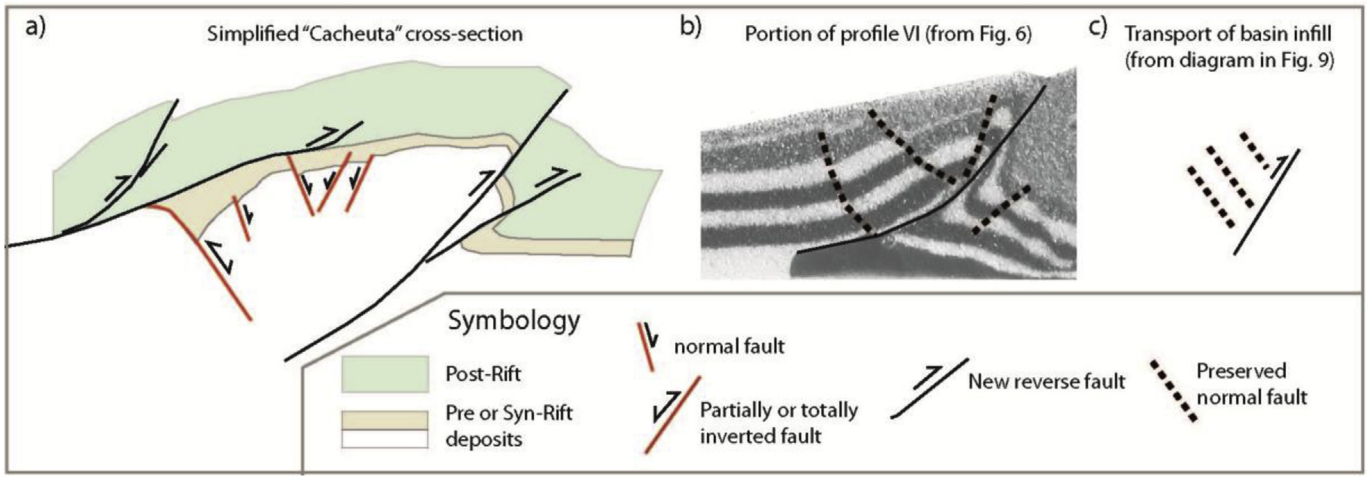

Fig. 12. Comparison between structures observed in a natural case (Cacheuta cross-section modified from Giambiagi et al., 2015) and in the widest zone (profile VI). The scheme for basin infill transport is the same from Fig. 9.

development are rooted at shallow depths, without necessarily involving basement (Fig. 13b). An example of the latter is the inverted Abanico Basin (Fig. 1) in the Principal Cordillera of central Chile (c. 32°-35°S, Charrier et al., 2005), where footwall rocks were deformed by means of new reverse faults. This fact was also observed by Pinto et al. (2010), who suggested that major uplift was accommodated by new reverse faults during inversion of a basin without pre-defined margins (Fig. 13a).

4.2.5. Backthrusts and shortcuts

In both models, compression allowed the generation of new reverse faults, which accommodated shortening by means of, among other structures, backthrusts and shortcuts. The backthrusts were especially important in the wider zone of the basin, mainly in model B (Profile IX in Fig. 9), with an equal amount of compression regarding extension. Conversely, shortcuts were more important in the narrow basin zone of model A (profiles IV and V in Fig. 9), where the amount of compression greatly exceeds the amount of extension (Rse > 1). These structures are commonly present in natural examples. These same features have been modeled previously to explain the structural evolution of the Southern Patagonian Andes (Likerman et al., 2013) supporting the hypothesis of homogeneous inversion on an asymmetrical basin, as in Model A of this work. In this context, such a configuration could likely correspond to the innermost zone of a pre-existing basin of variable width.

Similarly, the development of shortcuts in basin inversion models was also indicated by Pinto et al. (2010) and also by Muñoz-Sáez et al. (2014). Therein, the development of footwall shortcuts rooted out of the normal faults positively border of reactivated (Fig. 13b) was associated with high sedimentation within the basin. In our study, which considered completely filled basins previous to the inversion phase, shortcuts were produced where the basin was narrowest. Thus, our results complement previous studies (Pinto et al., 2010) suggesting that footwall deformation in an inverted basin setting is conditioned not only by high sedimentation within the basin, but also by the narrowness of the basin, where shortening magnitudes can easily be higher than the amount of extension.

4.2.6. Oblique strike structures and/or rotation

In Model A, the *pop-up* structure is controlled by reverse faults, of a slightly oblique orientation, related to the north to south variation of the basin width. The presence of oblique structures, beyond the basin margins in the narrow zone (Fig. 14), has been compared to the northernmost segment of the Abanico basin (e.g., Charrier et al., 2002) exposed in the Principal Cordillera of central Chile at c. 32°S (e.g., Jara et al., 2015). In this area, oblique NNW-SSE trending thrusts of the La Ramada Fold-and-Thrust belt (e.g., Cristallini and Ramos, 2000) cut easternmost rocks of the Abanico basin, which suffered previous deformation related to N-S trending structures, interpreted as extensional-related faults (Jara and Charrier, 2014). Depocenters of the Abanico basin appear to be of

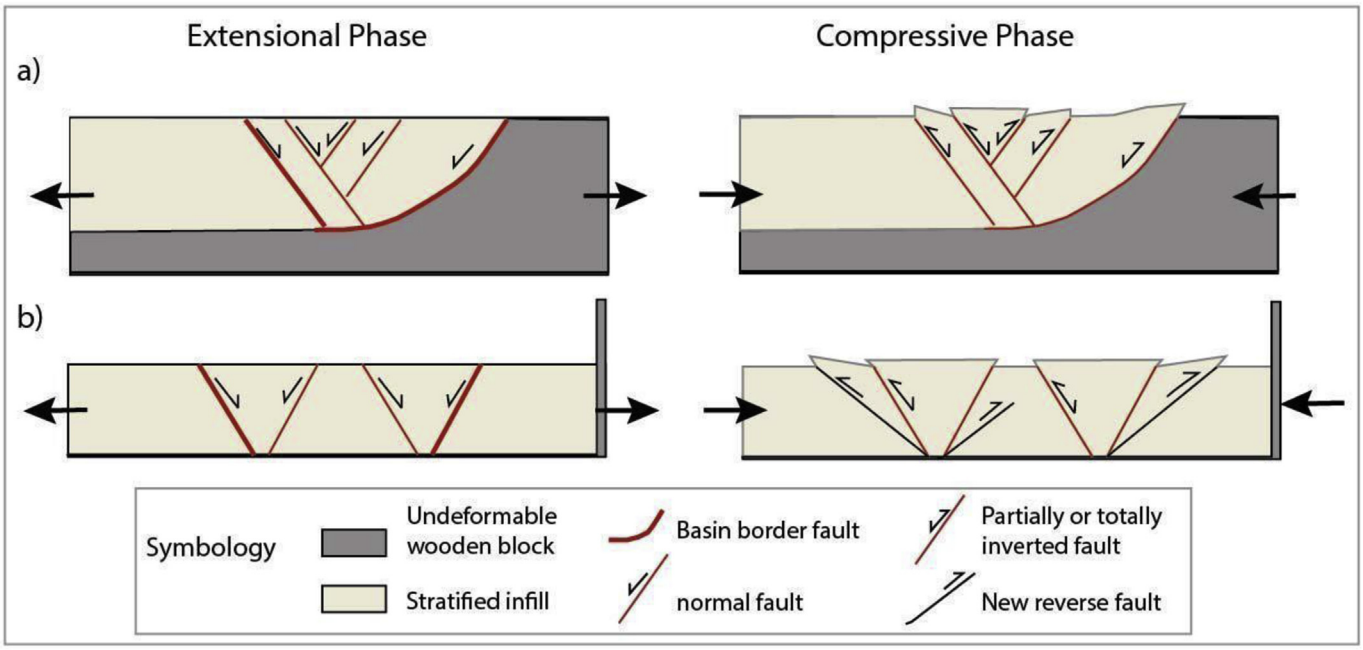

Fig. 13. Schematic diagrams of the resulting structure of inverted basins in analogue models. a) Simplified model that involved pre-defined faults, b) Simplified model without pre-defined faults.

a reduced development in comparison to the ones identified at southern latitudes (e.g., Charrier et al., 2002; Muñoz-Sáez et al., 2014; Tapia, 2015; Piquer et al., 2017). The latter is consistent with the results of Model A, where non-rotational oblique reverse faults are generated where Rse>1 (narrow zone of the basin). Moreover, this comparison is consistent with little or null block rotations registered at the Principal Cordillera of central Chile, north of 33° S, evidenced by paleomagnetic data provided by Arriagada et al. (2013). Jara et al. (2015) points out that a significant amount of rotation is required to generate oblique structures in models with no variations in the width of the pre-existing basin.

On the other hand, in model B, the same type of basin was inverted by progressively variating the convergence vector by rotation. We observed rotation of fault bounded blocks during the compressive phase, which implies that structurally bounded blocks should preserve a paleomagnetic signature related to rotation about a vertical axis (e.g., Costa and Speranza, 2003). There are cases of natural inversion processes, where paleomagnetic data records significant rotation during the closure of a basin. An example of the latter is the Rocas Verdes back-arc basin of the southernmost Andes (e.g., Diraison et al., 2000; Eagles, 2016), with evidence of significant counter-clockwise rotations coeval to basin closure during the evolution of the Patagonian orocline (Poblete et al., 2014, 2016; Torres Carbonell et al., 2016).

5. Concluding remarks

In this study, we show how the closure style of a heterogeneously extended basin influences the final geometry of the structures resulting from inversion. The analysis of our modeling results, their interpretation and comparisons with natural prototypes has led to the following concluding remarks:

- The pre-existing geometry of an extensional basin influences geometrically and kinematically the tectonic inversion process, as it controls the main characteristics (distribution, geometry and vergence) of the structures generated during contraction subsequent to extension (inversion). This idea is strengthened by the fact that the main differences regarding models of inversion of symmetrical basins are due to the geometry of the basin, and the location and orientation of the normal faults controlling basin development.

- Most of the contractional deformation imposed in the models is absorbed in the interiors of the basin. However, when the amount of shortening surpasses the amount of extension, deformation is propagated outside the basin, allowing the generation of oblique-trending reverse faults, and prompting a progressively major uplift in areas where basin development was minor. These structures were generated as oblique faults, and did not experienced rotation during inversion. On the other hand, N-S striking structures are generated in both types of models, mainly in the interiors of the basin, even when inversion was produced by means of differential compression. The latter closure mechanism allows rotation of the sedimentary infill within the inverted basin.

- Major contrasts were observed with respect to basin inversion models that pre-define the location and orientation of inherited structures, by including rigid blocks simulating basement rocks. As our models did not consider a pre-faulted basement, we suggest to compare the results of this study to basins that have experienced extension related to shallow detachment levels, where the developed structural style is thin-skinned.
- We adopt the term “doubly-vergent inverted basins” given the features observed in our models, showing reverse structures of an opposite vergence. Zones in which depocenters are “extruded” by means of a pop-up structure could actually correspond to areas close to the bordering structures in a natural prototype. In some cases, when shortening is greater than extension (Rse>1), shortcuts and new reverse faults are dominant. The opposite vergence (towards the basin interior) occurs in both models, but mainly in the zone where the basin is widest. Also in the widest zones, when Rse$\leq$1, backthrusts become dominant.

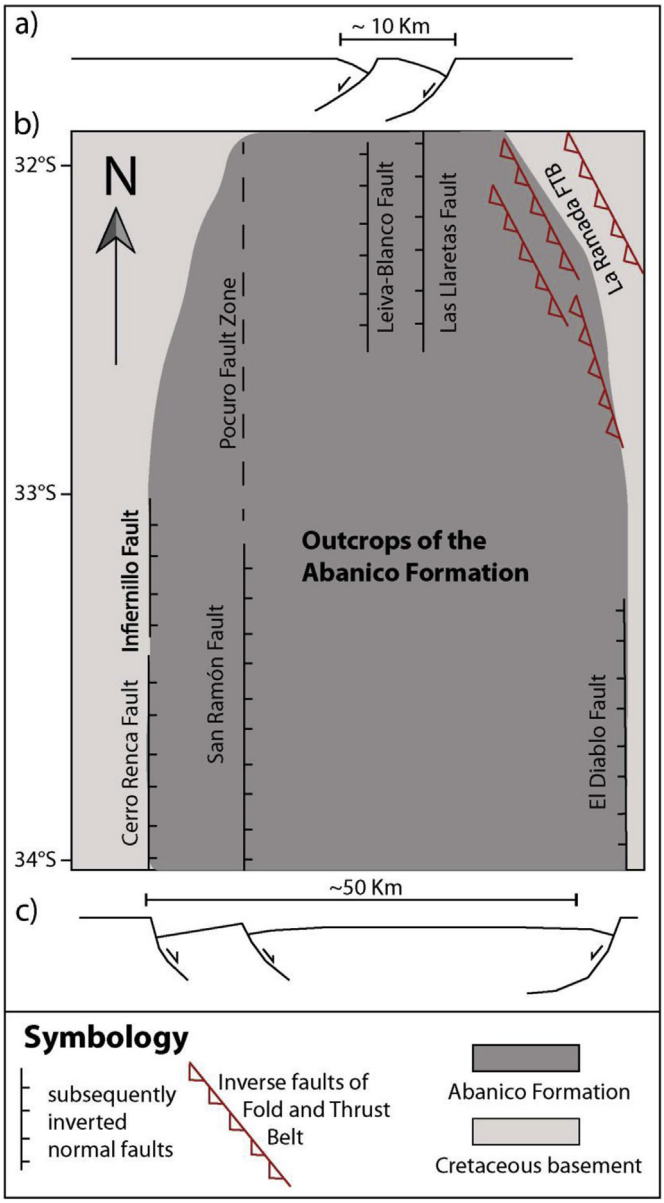

Fig. 14. Outcrops of the Abanico basin between 32° and 34°S, and some of the structures that have controlled its formation and subsequent deformation. We highlight the oblique trending faults (red) of the FPC La Ramada towards the northeastern end of the basin, between 32° and 33 °S. a) and c) Schematic profiles highlighting basin width at 32° and 34° respectively, showing some interpreted master faults. b) Schematic distribution of the Abanico Formation and related structures in plan-view (Modified from Jara et al., 2015). (For interpretation of the references to colour in this figure legend, the reader is referred to the web version of this article.)

- By recognizing the analyzed structural elements of this contribution in natural inverted basins, we can indirectly infer the location of the structural element regarding the geometry of the previous basin (interiors, margins or surroundings), and/or the type of closure responsible for inversion of the extensional system.
- The main characteristics of the performed analogue models are comparable to features of natural Andean inverted extensional basins. We propose that our results can also be applied to other inverted basins, similar to the Andean tectonic setting, to understand the influence of the original geometry of the basin in its final inverted geometry and its uplift variations.

Acknowledgments

This contribution was developed in the context of the DICYT 051615JM Proyect, funded by VRIDEI (Vicerrectoría de Investigación, Desarrollo e Innovación) of University of Santiago de Chile (USACH). We sincerely acknowledge Ernesto Cristallini and Matias Ghiglione, for their constant support in the Laboratory of Geological Modeling (LaMoGe) at University of Buenos Aires (UBA, Argentina), during the experimental runs and analysis, interpretation, and discussion of the model results. Thorough revisions of the original manuscript, performed by an anonymous reviewer and F. Martínez (UCN, Chile), greatly enhanced the quality of the text and figures presented in this work.

References

Amilibia, A., Sàbat, F., McClay, K.R., Muñoz, J.A., Roca, E., Chong, G., 2008. The role of inherited tectono-sedimentary architecture in the development of the central Andean mountain belt: insights from the Cordillera de Domeyko. J. Struct. Geol. 30, 1520–1539.

Armijo, R., Rauld, R., Thiele, R., Vargas, G., Campos, J., Lacassin, R., Kausel, E., 2010. The west andean thrust (WAT), the san ramón fault and the seismic hazard for Santiago (Chile). Tectonics 29, TC2007. https://doi.org/10.1029/2008TC002427.

Arriagada, C., Ferrando, R., Córdova, L., Morata, D., Roperch, P., 2013. The Maipo Orocline: a first scale structural feature in the Miocene to Recent geodynamic evolution in the central Chilean Andes. Andean Geol. 40 (3), 419–437. https://doi.org/10.5027/andgeoV40n3-a02.

Bechis, F., Giambiagi, L.B., Lanés, S., García, V.H., Tunik, M.A., 2009. Evidencias de extensión oblicua en los depósitos de sinrift del sector norte de la cuenca neuquina. Rev. Asoc. Geol. Argent. 65, 293–310.

Bechis, F., Cristallini, E., Giambiagi, L., Yagupsky, D., Guzmán, C., García, V., 2014. Transtensional tectonics induced by oblique reactivation of previous lithospheric anisotropies during the Late Triassic to Early Jurassic rifting in the Neuquén basin: insights from analog models. J. Geodyn. 79, 1–17. https://doi.org/10.1016/j.jog.2014.04.010.

Bonini, M., Sani, F., Antonielli, B., 2012. Basin inversion and contractional reactivation of inherited normal faults: a review based on previous and new experimental models. Tectonophysics 522–523, 55–88. https://doi.org/10.1016/j.tecto.2011.11.014.

Brun, J.P., Nalpas, T., 1996. Graben inversion in nature and experiments. Tectonics 15, 677–687. https://doi.org/10.1029/95TC03853.

Buchanan, P.G., McClay, K.R., 1991. Sandbox experiments of inverted listric and planar fault systems. In: Cobbold, P.R. (Ed.), Experimental and Numerical Modelling of Continental Deformation. Tectonophysics, vol. 188, pp. 97–115.

Carrapa, B., Reyes-Bywater, S., Safipour, R., Sobel, E.R., Schoenbohm, L., DeCelles, P.G., Reiners, P.W., Stockli, D., 2014. The effect of inherited paleotopography on exhumation of the Central Andes of NW Argentina. Geol. Soc. Am. Bull. 126, 1–2, 66-77.

Carrera, N., Muñoz, J.A., Sabat, F., Roca, E., Mon, R., 2006. The role of inversion tectonics in the structure of the Cordillera Oriental (NW Argentinean Andes). J. Struct. Geol. 28, 1921–1932.

Charrier, R., Baeza, O., Elgueta, S., Flynn, J., Gans, R., Kay, S., Muñoz, N., Wyss, A., Zurita, E., 2002. Evidence for Cenozoic extensional basin development and tectonic inversion south of the flat-slab segment, southern Central Andes, Chile (33°–36°S). J. S. Am. Earth Sci. 15, 117–139.

Charrier, R., Bustamante, M., Comte, D., Elgueta, E., Flynn, J., Iturra, I., Muñoz, N., Pardo, M., Thiele, R., Wyss, A., 2005. The Abanico extensional basin: regional extension, chronology of tectonic inversion and relation to shallow seismic activity and Andean uplift. Neues Jahrb. für Geol. Palaontologie- Abh. 1–2, 43-77.

Charrier, R., Pinto, L., Rodríguez, M.P., 2007. Tectonostratigraphic evolution of the andean orogen in Chile. In: Geological Society Special Publication: the Andes of Chile, pp. 21–114.

Charrier, R., Ramos, V.A., Tapia, F., Sagripanti, L., 2015. In: Tectono-stratigraphic Evolution of the Andean Orogen between 31 and 37 S (Chile and Western Argentina), vol. 399. Geological Society, London, Special Publications, pp. 13–61 (1).

Corti, G., 2003. Transition from continental break-up to punctiform seafloor spreading: how fast, symmetric and magmatic. Geophys. Res. Lett. 30, 1–4. https://doi.org/10.1029/2003GL017374.

Costa, E., Speranza, F., 2003. Paleomagnetic analysis of curved thrust belts reproduced by physical models. J. Geodyn. 36, 633–654. https://doi.org/10.1016/j.jog.2003.08.003.

Coward, M.P., Gillcrist, R., Trudgill, B., 1991. Extensional structures and their tectonic inversion in the Western Alps. In: Roberts, A.M., Yielding, G., Freeman, B. (Eds.), The Geometry of Normal Faults, Geological Society Special Publication, vol. 56, pp. 93–113.

Cristallini, E.O., Ramos, V.A., 2000. Thick-skinned and thin-skinned thrusting in the La Ramada fold and thrust belt: crustal evolution of the High Andes of San Juan, Argentina (32° LS). Tectonophysics 317, 205–235. https://doi.org/10.1016/

S0040-1951(99) 00276–0.
Dalziel, I.W.D., 1981. Back-arc extensión in the Southern Andes – a review and critical reappraisal. Philosophical Trans. R. Soc. A – Math. Phys. Eng. Sci. 300 (1454), 319–335.
Davy, P., Cobbold, P.R., 1991. Experiments on shortening of a 4-layer model of the continental lithosphere. Tectonophysics 188 (1–2), 1–25.
Diraison, M., Cobbold, P., Gapais, D., Rossello, E.A., Le Corre, C., 2000. Cenozoic crustal thickening, wrenching and rifting in the foothills of the southernmost Andes. Tectonophysics 316, 91–119.
Dubois, A., Odonne, F., Massonnat, G., Lebourg, T., Fabre, R., 2002. Analogue modelling of fault reactivation: tectonic inversion and oblique remobilisation of grabens. J. Struct. Geol. 24, 1741–1752. https://doi.org/10.1016/S0191-8141(01) 00129-8.
Eagles, G., 2016. Plate kinematics of the Rocas Verdes basin and patagonian orocline. Gondwana Res. 37, 98–109. https://doi.org/10.1016/j.gr.2016.05.015.
Eubank, R.T., Makki, A.C., 1981. Structural Geology of the Central Sumatra Back-arc Basin. Indonesian Petroleum Association, pp. 153–196, 10th Anniversary Convention.
Faccenna, C., Nalpas, T., Brun, J.P., Davy, P., Bosi, V., 1995. The influence of pre-existing thrust faults on normal fault geometry in nature and in experiments. J. Struct. Geol. 17, 1139–1149. https://doi.org/10.1016/0191-8141(95)00008-2.
Farías, M., Charrier, R., Carretier, S., Martinod, J., Fock, A., Campbell, D., Cáceres, J., Comte, D., 2008. Late Miocene high and rapid surface uplift and its erosional response in the Andes of central Chile (33°-35° S). Tectonics 27, TC1005.
Farías, M., Comte, D., Charrier, R., Martinod, J., David, C., Tassara, A., Tapia, F., Fock, A., 2010. Crustal scale structural architecture in central Chile based on seismicity and surface geology: implications for Andean mountain building. Tectonics 29, TC3006.
Giambiagi, L.B., Ramos, V.A., Godoy, E., Alvarez, P.P., Orts, S., 2003. Cenozoic deformation and tectonic style of the Andes, between 33 and 34 south latitude. Tectonics 22 (4). https://doi.org/10.1029/2001TC001354.
Giambiagi, L.B., Mescua, J., Bechis, F., Tassara, A., Hoke, G., 2012. Thrust belts of the southern Central Andes: along-strike variations in shortening, topography, crustal geometry, and denudation. Geol. Soc. Am. Bull. 124 (7–8), 1339–1351.
Giambiagi, L.B., Spagnotto, S., Moreiras, S., Gómez, G., Stahlschmidt, E., Mescua, J.F., 2015. Three-dimensional approach to understanding the relationship between the Plio-Quaternary stress field and tectonic inversion in the Triassic Cuyo Basin, Argentina. Solid earth 6, 747–763.
Herrera, S., Pinto, L., Farías, M., Yagupsky, D., Guzmán, C., Charrier, R., 2017. Analogue Modeling of Rotational Orogenic Wedges: Implications for the Neogene Structural Evolution of the Southern Central Andes (33°-35°S). Abstract 243934 presented at 2017 Fall Meeting. AGU, New Orleans, LA, pp. 11–15. Dec.
Hubbert, M.K., 1937. Theory of scaled models as applied to the study of geological structures. Geol. Soc. Am. Bull. 48, 1459–1520.
Hubbert, M.K., 1951. Mechanical basis for certain familiar geologic structures. Geol. Soc. Am. Bull. 62, 355–372.
Huyghe, P., Mugnier, J.L., 1992. The influence of depth on reactivation in normal faulting. J. Struct. Geol. 14, 991–998. https://doi.org/10.1016/0191-8141(92) 90030-Z.
Isacks, B.L., 1988. Uplift of the central andean plateau and bending of the bolivian orocline. J. Geophys. Res. 93 (B4), 3211–3231.
Jara, P., Charrier, R., 2014. Nuevos antecedentes estratigráficos y geocronológicos para el Meso-Cenozoico de la Cordillera Principal de Chile entre 32° y 32°30S: implicancias paleogeográficas y estructurales. Andean Geol. 41 (1), 174–209. https://doi.org/10.5027/andgeoV41n1-a07.
Jara, P., Likerman, J., Winocur, D., Ghiglione, M.C., Cristallini, E.O., Pinto, L., Charrier, R., 2015. Role of basin width variation tectonic inversion: insight from analogue modelling and implications for the tectonic inversion of the Abanico Basin, 32°-34° S, Central Andes. In: Sepúlveda, S.A., Giambiagi, L.B., Moreiras, S.M., Pinto, L., Tunik, M., Hoke, G.D., Farías, M. (Eds.), Geodynamic Processes in the Andes of Central Chile and Argentina, vol. 399. Geological Society, London, Special Publications, pp. 83–107. https://doi.org/10.1144/SP399.7.
Jordan, T., Isacks, B., Allmendinger, R.W., Brewer, J.A., Ramos, V.A., Ando, C.J., 1983. Andean tectonics related to geometry of subducted Nazca plate. Geol. Soc. Am. Bull. 94, 341–361.
Van Keken, P.E., Spiers, C.J., Van den Berg, A.P., Muyzert, E.J., 1993. The effective viscosity of rocksalt: implementation of steady-state creep laws in numerical models of salt diapirism. Tectonophysics 225 (4), 457–476.
Kozlowski, E., Manceda, R., Ramos, V., 1993. Estructura. In: Ramos, V. (Ed.), Geologıa y Recursos Naturales de Mendoza. Relatorio del XII Congreso Geologico Argentino y II Congreso de Exploración de Hidrocarburos, pp. 235–256.
Likerman, J., Burlando, J.F., Cristallini, E.O., Ghiglione, M.C., 2013. Along-strike structural variations in the Southern Patagonian Andes: insights from physical modeling. Tectonophysics 590, 106–120. https://doi.org/10.1016/j.tecto.2013.01.018.
Lowell, J.D., 1995. In: Mechanics of Basin Inversion from Worldwide Examples, vol. 88. Geological Society, London, Special Publications, pp. 39–57 (1).
Marques, F.O., Nogueira, C.R., 2008. Normal fault inversion by orthogonal compression: sandbox experiments with weak faults. J. Struct. Geol. 30 (6), 761–766.
Martínez, F., Cristallini, E., 2017. The doubly vergent inverted structures of the Mesozoic basins of northern Chile (28°S): a comparative analysis from field data and analogue modeling. J. S. Am. Earth Sci. 77, 327–340. https://doi.org/10.1016/j.jsames.2017.02.002.
Martínez, F., Arriagada, C., Peña, M., Del Real, I., Deckart, K., 2012. The structure of the Chañarcillo Basin: an example of tectonic inversion in the Atacama region, northern Chile. J. S. Am. Earth Sci. 42, 1–16. https://doi.org/10.1016/j.jsames.2012.07.001.
Martínez, F., Arriagada, C., Valdivia, R., Deckart, K., Peña, M., 2015. Geometry and kinematics of the andean thick-skinned thrust systems: insights from the chilean frontal Cordillera (28°-28.5°S), central Andes. J. S. Am. Earth Sci. 64, 307–324. https://doi.org/10.1016/j.jsames.2015.05.001.
McClay, K.R., 1995. The geometries and kinematics of the inverted fault Systems: a review of analogue model studies. In: Buchanan, J.G., Buchanan, P.G. (Eds.), Basin Inversion, vol. 88. Geological Society of London Special Publication, pp. 97–118.
McClay, K., Buchanan, P.G., 1992. Thrust faults in inverted extensional basins. In: McClay, K.R. (Ed.), Thrust Tectonics. Chapman and Hall, London, pp. 93–104.
Mescua, J.F., Giambiagi, L.B., Tassara, A., Gimenez, M., Ramos, V.A., 2014. Influence of pre-Andean history over Cenozoic foreland deformation: structural styles in the Malargüe fold-and-thrust belt at 35 S, Andes of Argentina. Geosphere 10 (3), 585–609.
Mescua, J.F., Giambiagi, L., Ramos, V.A., 2016. Los movimientos Andinos de Groeber y la evolución tectónica de Los Andes Centrales del Sur. Rev. Asoc. Geol. Argent. 74 (1), 49–58.
Muñoz-Sáez, C., Pinto, L., Charrier, R., Nalpas, T., 2014. Influence of depositional load on the development of a shortcut fault system during the inversion of an extensional basin: the Eocene-Oligocene Abanico Basin case, central Chile Andes (33°-35°S). Andean Geol. 41 (1), 1–28. https://doi.org/10.5027/andgeoV41n1-a01.
Nemčok, M., Mora, A., Cosgrove, J., 2013. In: Thick-skin-dominated Orogens; from Initial Inversion to Full Accretion: an Introduction, vol. 377. Geological Society, London, Special Publications, pp. 1–17 (1).
Oncken, O., Hindle, D., Kley, J., Elger, K., Victor, P., Schemann, K., 2006. Deformation of the Central Andean upper plate system – facts, fiction and constraints for plateau models. In: Oncken, O., Chong, G., Franz, G., Giese, P., Gotze, H.J., Ramos, V.A., Strecker, M.R., Wigger, P. (Eds.), The Andes – Active Subduction Orogeny. Springer, Berlin, pp. 3–28.
Pinto, L., Muñoz, C., Nalpas, T., Charrier, R., 2010. Role of sedimentation during basin inversion in analogue modelling. J. Struct. Geol. 32, 554–565. https://doi.org/10.1016/j.jsg.2010.03.001.
Piquer, J., Hollings, P., Rivera, O., Cooke, D., Baker, M., Testa, F., 2017. Along-strike segmentation of the Abanico Basin, central Chile: new chronological, geochemical and structural constraints. Lithos 268–271, 174–197. https://doi.org/10.1016/j.lithos.2016.10.025.
Poblete, F., Roperch, P., Hervé, F., Diraison, M., Espinoza, M., Arriagada, C., 2014. The curved Magallanes fold and thrust belt: tectonic insights from a paleomagnetic and anisotropy of magnetic susceptibility study. Tectonics 33 (12), 2526–2551. https://doi.org/10.1002/2014TC003555.
Poblete, F., Roperch, P., Arriagada, C., Ruffet, G., Ramırez de Arellano, C., Hervé, F., Poujol, M., 2016. Late cretaceous – early eocene counterclockwise rotation of the fueguian Andes and evolution of the patagonia-antarctic peninsula system. Tectonophysics 668–669, 15–34. https://doi.org/10.1016/j.tecto.2015.11.025.
Pose, F., Spagnuolo, M., Folguera, A., 2005. Modelo para la variación del volumen orogénico andino y acortamientos en el sector 20°-46°S. Rev. Asoc. Geol. Argent. 60 (4), 724–730.
Ramberg, H., 1981. Gravity, Deformation and the Earth's Crust. Academic Press, London, p. 452.
Ramos, V.A., 2009. Anatomy and global context of the Andes: main geologic features and the Andean orogenic cycle. Geol. Soc. Am. Memoirs 204, 31–65.
Ramos, V.A., Cristallini, E.O., Pérez, D.J., 2002. The pampean flat-slab of the central Andes. J. S. Am. earth Sci. 15 (1), 59–78.
Ranalli, G., 2000. Rheology of the crust and its role in tectonic reactivation. J. Geodyn. 30 (1), 3–15.
Schellart, W.P., Strak, V., 2016. A review of analogue modelling of geodynamic processes: approaches, scaling, materials and quantification, with and application to subduction experiments. J. Geodyn. 100, 7–32. https://doi.org/10.1016/j.jog.2016.03.009.
Sibson, R.H., 1985. A note on fault reactivation. J. Struct. Geol. 7, 751–754. https://doi.org/10. 1016/0191–8141(85)90150-6.
Soto, R., Casas-Sainz, A.M., Pueyo, E.L., 2006. Along-strike variation of orogenic wedges associated with vertical axis rotations. Journal of Geophysical Research: Solid Earth 111 (B10).
Tapia, F., 2015. Evolución tectónica y configuración actual de los Andes Centrales del sur (34°45'-35°30' S). PhD Thesis. Universidad de Chile, p. 306. Unpublished.
Tassara, A., Götze, H.J., Schmidt, S., Hackney, R., 2006. Three-dimensional density model of the Nazca plate and the Andean continental margin. J. Geophys. Res. Solid Earth 111 (B9).
Torres Carbonell, P., Guzmán, C., Yagupsky, D., Dimieri, L., 2016. Tectonic models for the Patagonian orogenic curve (southernmost Andes): an appraisal based on analog experiments from the Fueguian thrust-fold belt. Tectonophysics 671, 76–94.
Turienzo, M.M., 2010. Structural style of the Malargüe fold-and-thrust belt at the diamante river area (34° 30′–34° 50′ S) and its linkage with the Cordillera frontal, Andes of central Argentina. J. S. Am. Earth Sci. 29 (3), 537–556.
Uliana, M.A., Arteaga, M.E., Legarreta, L., Cerdán, J.J., Peroni, G.O., 1995. Inversion Structures and Hydrocarbon Occurrence in Argentina. In: Geological Society, London, Special Publications, vol. 88, pp. 211–233 (1).
Weijermars, R., 1986. Finite strain of laminar flows can be visualized in SGM36-

polymer. Naturwissenschaften 73 (1), 33–34.
Weijermars, R., Jackson, M.T., Vendeville, B., 1993. Rheological and tectonic modeling of salt provinces. Tectonophysics 217 (1–2), 143–174.
Winocur, D.A., Litvak, V.D., Ramos, V.A., 2015. Geological Society, London, Special Publications Magmatic and tectonic evolution of the Oligocene Valle del Cura basin, main Andes of Argentina and Chile: evidence for generalized extension. In: Sepúlveda, S.A., Giambiagi, L.B., Moreiras, S.M., Pinto, L., Tunik, M., Hoke, G.D., Farías, M. (Eds.), Geodynamic Processes in the Andes of Central Chile and Argentina, vol. 399. Geological Society, London, Special Publications, pp. 109–130. https://doi.org/10.1144/SP399.2.
Yagupsky, D.L., Cristallini, E.O., Fantin, J., Valcarce, G., Bottesi, G., Varade, R., 2008. Oblique half-graben inversion of the Mesozoic Neuquén Rift in the Malargüe fold and thrust belt, Mendoza, Argentina: new insights from analogue models. J. Struct. Geol. 30, 839–853. https://doi.org/10.1016/j.jsg.2008.03.007.